Expanding the spectral responsiveness of photodetectors via the integration of TiO_2 and Y_2O_3 quantum dots prepared by laser ablation in liquid

M. A. Ali [a,*], G. Z. Alwan [b]
[a] *Applied Physics Department, College of Applied Science,University of Technology, Baghdad, Iraq*
[b] *Physics Department, Faculty of Science Mustansiriyah University, Baghdad, Iraq*

This research aims to improve the performance of photo detectors by fabricating and evaluating three types of Nano detectors based on titanium oxide (TiO_2) and yttrium oxide (Y_2O_3) using the laser ablation technique. The detectors were prepared according to the following compositions: Ag/ TiO_2 / n-Si/Ag, Ag/ Y_2O_3 / n-Si/Ag, Ag/ TiO_2 / Y_2O_3/n-Si/Ag, and were studied using XRD, FESEM, AFM, UV-Vis, FTIR, in addition to evaluating their performance through measurements of specific detectivity (D*) and spectral response (R). The results showed that the combination of TiO_2 and Y_2O_3in the Ag/ TiO_2/ Y_2O_3/n-Si/Ag detector performed the best in terms of specific detectivity and spectral response in (Ultraviolet, Visible and Near Infrared) range, making it the most efficient from other detectors. Its superiority is due to the cumulative effect of incorporating TiO_2 and Y_2O_3, which reduced the effective energy gap and improved the efficiency of photon absorption and electron transfer. Although TiO_2 showed good UV and NIR absorption but it has low absorption in the visible spectrum owing to its broad energy gap of 3.3 eV when used alone. The detector based on Y_2O_3alone in the Ag / Y_2O_3/n-Si/Ag did not yield significant improvement compared to the combination of TiO_2 and Y_2O_3in the Ag/ TiO_2/ Y_2O_3/n-Si/Ag detector, highlighting the role of Y_2O_3as a key material in enhancing the performance of photodetectors. This study confirms that yttrium oxide (Y_2O_3) is a promising material for the fabrication of highly efficient photodetectors due to its unique electronic and optical properties, which increases the sensitivity of the photodetector in (visible and near infrared) range. The outcomes also show that laser ablation technique is an effective approach for preparing nanomaterials with high precision, which enhances their structural and optical properties. Given these results, it may be recommended that amalgamation of TiO_2 and Y_2O_3 be adopted as a base material in the design of future photodetectors, with additional processing techniques being explored to improve the performance of TiO_2 and reduce its recombination rates. This study also opens up new avenues for the development of advanced nanophotodetectors with novel fabrication techniques, enhancing their applications in the fields of environmental sensing, optical communications, and advanced electronic.

(Received April 8, 2025; Accepted July 7, 2025)

Keywords: Photodetector, Laser ablation, Titanium dioxide, Yttrium dioxide, Spectral response, Specific detectivity

1. Introduction

Photodetectors are devices that can convert lights signals into electrical signals; it has wide ranging applications, including optical communication systems, environmental and biological sensors, and solar energy technologies. Improving the performance of photodetectors has become an active research area because the ever-increasing demand for more efficient and less expensive devices [1] . Here comes the importance of using nanomaterials, as the quantum properties of these materials can enhance the sensitivity of photodetectors and reduce noise, leading to improved overall performance [2]. Silicon is a widely used semiconductor with a narrow band gap of 1.12 eV that is

* Corresponding author: maryam.a.ali@uotechnology.edu.iq
https://doi.org/10.15251/DJNB.2025.203.769

ideal for creating broadband photodetectors [3]. Utilizing silicon as a photoelectric detection material has the benefits of being inexpensive and having a proven method for integrating devices [4]. However, silicon is an indirect band gap material, meaning that its photoelectron transition probability is lower than that of direct band gap semiconductors. This can have a significant impact on how well silicon-based photodetectors function. As a result, it has a modest ultraviolet (UV) reaction. Due to silicon's limited penetration depth, this problem is especially noticeable in the ultraviolet spectrum[5][6]. This can be overcome by forming a silicon heterojunction with wide-band gap semiconductors[7][8].Metal oxides such as ZnO[9],TiO_2[10],Ga2O3 [11], SnO2[12], MoO3 [13]and NiO[14], They are wide-band gap semiconductors and can be used to enhance the UV response of silicon [15][16]. For instance, a NiO_2/TiO_2/n-Si device fabricated using the magnetron sputtering method exhibited an excellent broadband detection range (341–1050 nm) and self-powered performance, with an EQE of 553% under zero bias[17]. A p-NiO/SiO2/n-ZnO device fabricated by the magnetron sputtering method demonstrated a high responsivity of 5.77 A/W and an EQE of 1.96×10^3 % under 365 nm light illumination, exhibiting a fast response time of 0.048 s [18]. A TiO_2-NPs/P-Si /Ag was fabricated using laser –assisted chemical bath deposition exhibited excellent (UV) light response with the current increasing by 138% when exposed to UV light at a wavelength of 385nm and showing sensitivity ranging from (0.15 e^{-3} to 2.06e^{-3})A/W[19] . Nanocrystalline SnO2-Y_2O_3 thin films prepared by the chemical bath deposition approach on SiO2/Si substrates achieved 2988% sensitivity and a responsivity of 3.247 A/W at a wavelength of 360 nm, with rapid response and recovery times[20]. Among these materials, titanium dioxide (TiO_2) and yttrium oxide (Y_2O_3) stand out as promising candidates due to their unique properties [22,23] . For example, TiO_2 is known for its wide energy gap of about (3.2 eV) for the anatase phase, which makes it ideal for absorbing ultraviolet rays. It is the perfect material for solar cell and photodetector applications because of its great chemical stability and capacity for photocatalysis [23][24] . However, Y_2O_3 is a semiconductor that can be used in optical and electrical applications due to its large energy gap of 5.5eV remarkable transparency in the visible and infrared spectrum makes it a perfect material for use in photodetectors and thin films [25] . Although TiO_2 and Y_2O_3have made significant strides in photodetectors, the majority of earlier research concentrated on their individual applications. To enhance photodetectors' performance, the impact of combining these materials into a multilayer structure must be investigated. In addition, the use of laser ablation technology to prepare nanoscale quantum dots has not been sufficiently explored in scientific literature. This technique allows the preparation of highly pure nanoparticles with a homogeneous size, which can enhance the properties of materials. This research aims to fabricate highly efficient photodetectors using TiO_2 and Y_2O_3 nano-quantum dots prepared by the laser ablation method. Three different compositions of the detectors were prepared: Ag/TiO_2/n-Si/Ag, Ag/Y_2O_3/n-Si/Ag, and Ag/TiO_2/ Y_2O_3 /n-Si/Ag to study the impact of each layer on the optical characteristics and overall performance of the detector. These detectors will be evaluated by measuring the spectral response at different wavelengths of light (λ), specific detectivity (D*) and detector responsivity (R).

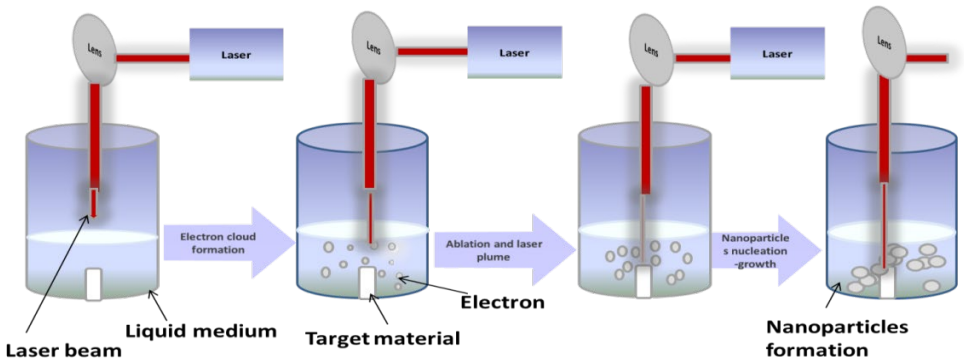

Fig. 1. Sketch of the laser ablation process.

2. Experimental parts

2.1. Preparation of (TiO_2 and Y_2O_3) NPs using laser ablation method

A preparation of TiO_2 and Y_2O_3 NPs performed by pulsed laser ablation of a high purity Ti and Y target in high purity deionized water (DI). Using a hydraulic press with 5 ton for 15 min, 5 g of high purity (99.9%) Ti and Y powder were placed in the pressing mold to prepare Ti and Y pellets with 1.5 cm diameter. The laser beam focused on a Ti and Y target was placed in a glass vessel with 50 ml of DI water. Nd:YAG laser with a wavelength of 1064nm.The number of laser pulses used for target ablation was 500 with the laser energy used for ablation is fixed at 600mJ and frequency 8HZ. Fig. (1) shows the steps the work.

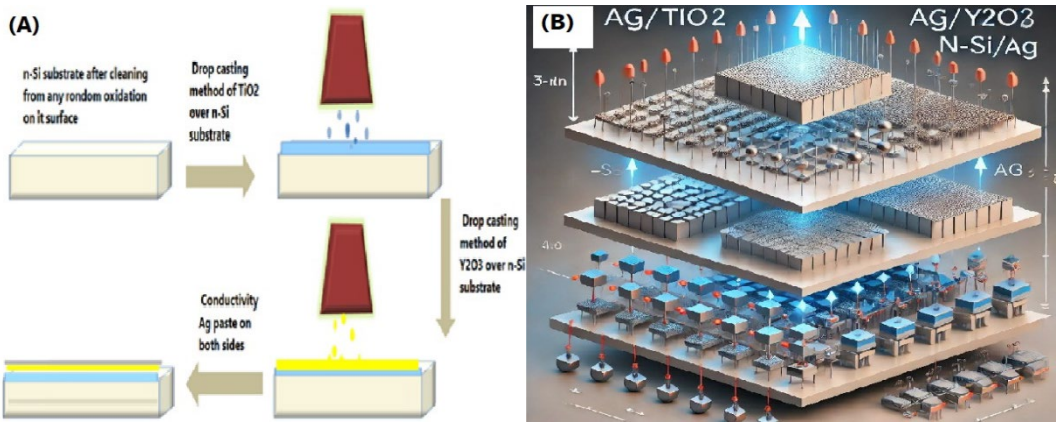

Fig. 2. Schematic diagrams illustrating the fabrication process of the Ag/TiO_2/Y_2O_3/n-Si/Ag photodetector.

2.2. Photodetectors deposition using (Drop Casting) method

The silicon (Si) substrate 1.5 x 1.5 cm^2 polished n-type was cleaned using ethanol and acetone in an ultrasonic bath for 15 min, and then dried by heating at 100°C. Thereafter, a Micropipette was used to drop a specific volume of the previously prepared nano-solution (TiO_2, Y_2O_3) at a rate of 20-50 mL on the substrate. Then the sample was gradually dried on a heating plate at (60-80)℃ to ensure that the material was distributed homogeneously on the surface of the substrate. Finally, Silver paste was used to create electrodes on the surface of the photodetector, where the electrodes were placed on both ends of the deposited nano-material to ensure effective electrical contact. The silver paste was dried at (100-150)℃ for (30) min to ensure good adhesion to the surface. Fig.(2) Shows the steps the work.

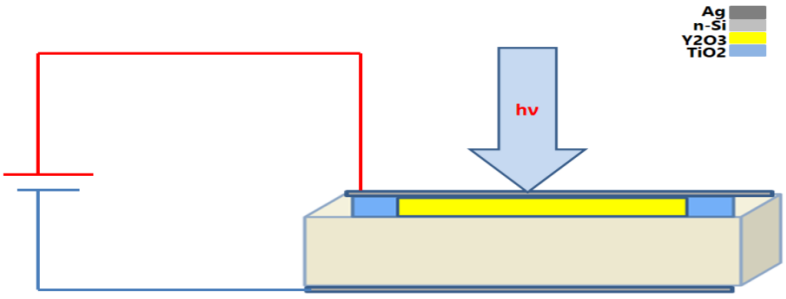

Fig. 3. Electrical circuit installation.

3. Description of the electrical circuit installation

Simple electrical circuit is designed as shown in the fig (3) to measure the photovoltaic response of the prepared reagents and the silver electrodes placed on the sample surface were connected to a connecting wires source of an external voltage source and a light source was used with a specific wavelength (UV-VIS LED). After connecting the electrical circuit, the photovoltaic response was registered when the sample was exposed to a light source. The current was measured by using a device (Keithley electrometer 2400) with load resistance (1KΩ) to turn the current into an effort. The characterization of the as-prepared TiO_2 and Y_2O_3 nanoparticles (NPs) was conducted using various analytical techniques. UV–visible spectrophotometry was carried out using a DU-8800D spectrophotometer (China) within the wavelength range of (190–1100) nm. FTIR spectra were recorded using an attenuated total reflection Fourier-transform infrared spectrophotometer (ATR-FTIR, ALPHA - BRUKER). The morphological properties of the TiO_2 and Y_2O_3 NPs were analyzed using Field Emission Scanning Electron Microscopy (FESEM, MIRA3 TESCAN). X-Ray Diffraction (XRD) patterns were recorded with a SHIMADZU XRD-6000 instrument (Japan) employing CuKα radiation (λ = 1.5406 Å). Atomic Force Microscopy (AFM) images were acquired using a Digital Instruments system (Nanoscope III and Dimension).

4. Results and discussion

Fig. (4) Shows the XRD examination of the TiO_2 sample, where sharp and narrow peaks appear, and indicating high crystallinity. The peak positions match the reference values for the anatase phase, which is one of the main phases of TiO_2. The highest apex appeared at 2θ = 25.35°, corresponding to the crystal plane (101), and is the most prominent peak in TiO_2 (anatase) according to the JCPDS 1272-21 card[26]. Other peaks at 2θ = 38.1°, 48.35°, 54.2°, 55.45°, 63.1°, 69.3°, 70.9°, and 75.4° corresponding to the (004), (200), (105), (211), (204), (116), (220), and (215) crystal planes, respectively, confirm that the material is in the pure anatase phase. The absence of peaks for the rutile and brookite phases indicates the purity of the phase in the prepared sample. The XRD examination of the Y_2O_3 sample shows sharp and strong peaks indicating a highly regular cubic crystal structure. The most intense peak appeared at 2θ = 29.2°, corresponding to the (222) crystal plane, which is the most prominent plane in Y_2O_3 as per the JCPDS 88-1040 card[26]. The presence of additional peaks at 2θ = 20.5°, 33.8°, 48.6°, 53.6°, and 58.0°, corresponding to the (211), (400), (440), (541), (622), and (631) planes, respectively, confirms that the sample crystallizes in the cubic crystal system. The results show that both samples possess a high crystallinity and regular distribution of atoms in the crystal lattice. The crystallite size of TiO_2 and Y_2O_3 was computed utilizing the Debye-Scherrer formula[27]:

$$D = \frac{0.94\lambda}{\beta\cos\theta} \tag{1}$$

where χ is the wavelength of the X-ray (1.5406 Å) for CuKα radiation, β is the full width at half maximum, and Θ is the peak position. The average crystallite size was determined to be 16.13 nm for TiO_2 and 13.6 nm for Y_2O_3. Table 1 summarizes the XRD analysis and calculated parameters for TiO_2 and Y_2O_3.

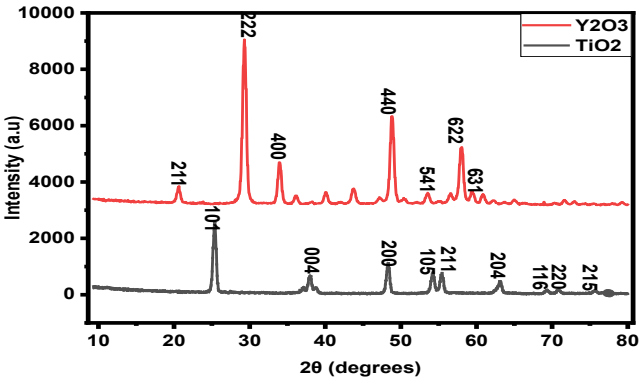

Fig. 4. X-ray diffraction pattern of TiO_2 and Y_2O_3.

Table 1. XRD Analysis and calculation of various parameters for TiO_2 and Y_2O_3 NPs.

	Sr No.	2θ (Deg.)	FWHM (Deg.)	FWHM (radians.)	d_{hkl}.(Å)	hkl	G.S (nm)	For unit cell edges: (TiO_2) a = b ≠ c /(Y_2O_3)a=b=c(Å)
TiO_2	1	25.35	0.4848	0.008505	3.5106	101	16.8	a ≈ 3.762 c ≈ 9.49
	2	38.1	0.5570	0.009772	2.3600	004	15.1	
	3	48.35	0.3488	0.006119	1.8810	200	25.0	
	4	54.25	0.8824	0.015481	1.6895	105	10.1	
	5	55.45	0.5335	0.00936	1.6557	211	16.8	
	6	63.1	0.7181	0.012598	1.4722	204	13.0	
Y_2O_3	1	20.5	0.534	0.009368	4.3289	211	15.1	a ≈10.54
	2	29.22	0.97	0.000384	3.0539	222	8.5	
	3	33. 8	0.67	0.009351	2.65	400	12.39	
	4	48.6	0.35	0.00614	1.8719	440	24.9	
	5	53.6	0.83	0.01456	1.7084	541	10.7	
	6	58.0	0.867	0.015211	1.5889	622	10.5	

The FTIR technique was utilized to analyze the chemical bonds and identify the functional groups present in the TiO_2 and Y_2O_3 compounds, as illustrated in Fig. (5). The synthesis of TiO_2 is confirmed by the absorption peak at 709 cm^{-1}, which is attributed to the (Ti-O) bond stretching vibration. Additionally, a peak at 1633 cm^{-1} appeared, which is ascribed to the (H-O-H) bending vibrations, reflecting the surface vibrations of water molecules. The peaks at 2857 cm^{-1} and 2925 cm^{-1} are likely due to organic residues from the preparation process and are related to (C-H) vibrations. The broad peak at 3431 cm^{-1} indicates the stretching vibrations of the (O-H) group, suggesting the presence of hydroxyl groups adsorbed on the surface [28][29]. The stretching vibrations at 572 cm^{-1}, attributed to the(Y-O) bond, confirmed the formation of Y_2O_3. In addition, peaks at 1114 cm^{-1} appear which may be due to the adsorption of inorganic impurities or (Y-O-Y) vibrations. Finally, a peak was observed at 1626 cm^{-1}, indicating water absorption, which is attributed to (H-O-H) bending vibrations [30][31].

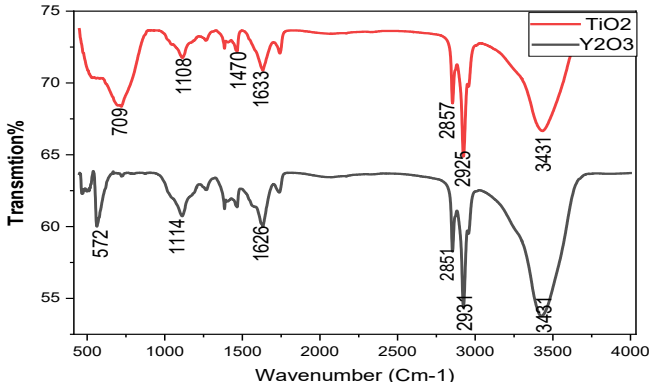

Fig. 5. FTIR spectrum for TiO_2 and Y_2O_3.

The (FESEM) image in Fig. (6) shows a cluster of nanoparticles that appear semi-spherical and multifaceted, with a tendency to aggregate. Some of the particles were measured using ImageJ software, revealing that most particles range between 30–40 nm in size. This relatively narrow distribution indicates good size homogeneity among the nanoparticles, as the smaller nanosize enhances the total surface area and leads to improved optical properties of the sample. In the image of TiO_2 in Fig. (7), the nanoparticles appear agglomerated with relatively larger sizes compared to Y_2O_3, with an average size estimated between 60–80 nm. The differences in average size between the two samples reflect the nature of the target material used in laser ablation. The smaller particles of the Y_2O_3 sample show higher surface activity, while the larger size of TiO_2 can provide distinctive photocatalytic properties. In both samples, the particles appear somewhat aggregated, which is common in nanomaterials due to high surface energy and reduced free surface area.

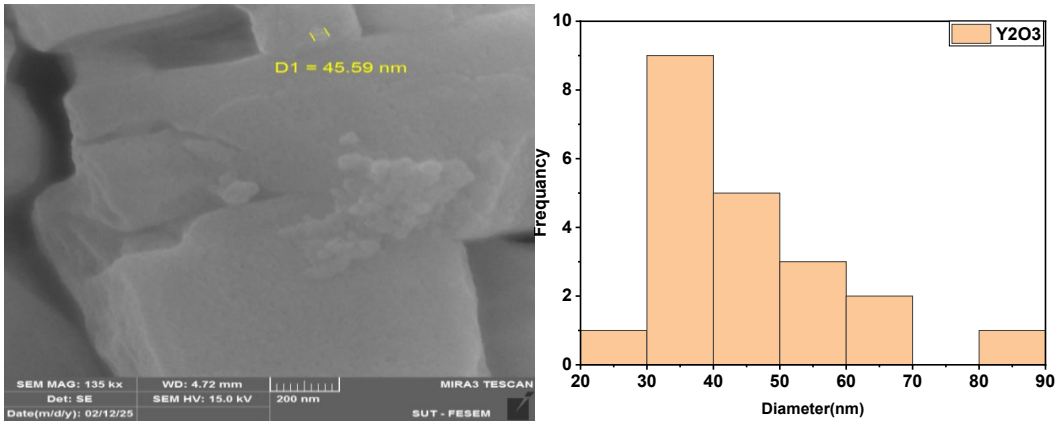

Fig. 6. FE-SEM image and histogram of particle size distribution of Y_2O_3.

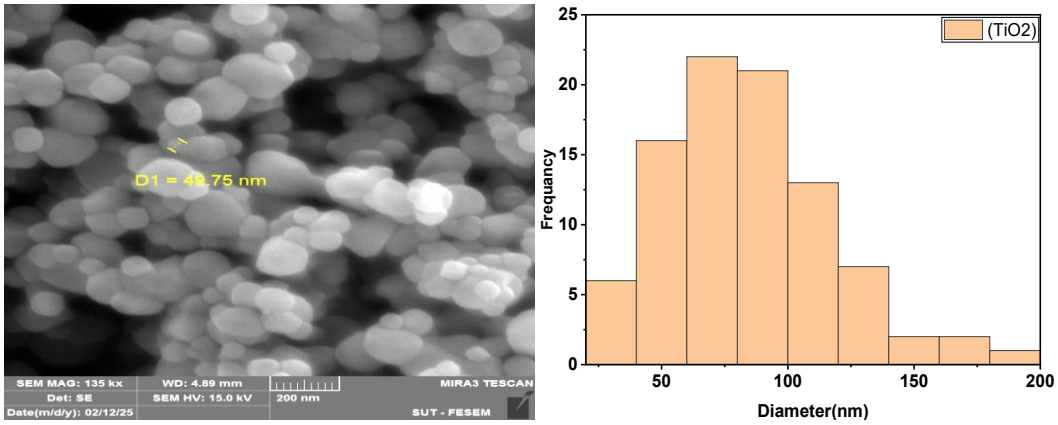

Fig. 7. FE-SEM image and histogram of particle size distribution of TiO_2.

The topographic properties of both TiO_2 and Y_2O_3 were analyzed using (AFM). Fig. (8-B) shows the surface topography of TiO_2, where the surface is characterized by relatively regular peaks and pits, with slight variation in heights, reflecting a homogeneous surface. The TiO_2 surface has a highly regular nanostructure with a root mean square roughness (RMS Roughness, Sq) = 2.44 nm and an average roughness (Sa) = 1.65 nm, indicating a relatively uniform distribution of nanoparticles. The material also recorded a maximum topographic height (Sz) = 37.72 nm, reflecting a nanoscale surface with limited height variations. The surface of this material limits the propagation of light within it, which reduces the sensitivity of TiO_2 as a photodetector compared to Y_2O_3. In addition, the small effective surface area (431,313 nm^2) means there are a few active sites to interact with light , which may reduce the efficiency of the photodetection [32][33]. In contrast, the AFM results of Y_2O_3, as shown in Fig. (7-A), showed that the surface of Y_2O_3 is described by more distinct peaks and a uniform distribution of nanoparticles, with distinct height variations and substantially increased roughness values. The Sa value was about3.00 nm, SQ about3.95nm, while Sz reached 43.31 nm. These values reflect greater variation in the height of the nanoparticles and more complex spectra leading to light absorption due to increased effects of internal reflections and optical scattering effects. Furthermore, Y_2O_3 provides a greater number of active sites for radiation detection due to its larger effective surface area(653,939 nm^2) , making it highly efficient in photodetector [31]. According to the results of scanning electron microscopy (FESEM) and XRD data, Y_2O_3 has a more complex and porous nanostructure and a more stable crystal structure compared to TiO_2, which enhances its interaction with light radiation and increases the efficiency of photodetection , making it a contributor to improving the material for light detection, as well as reducing noise in application systems.

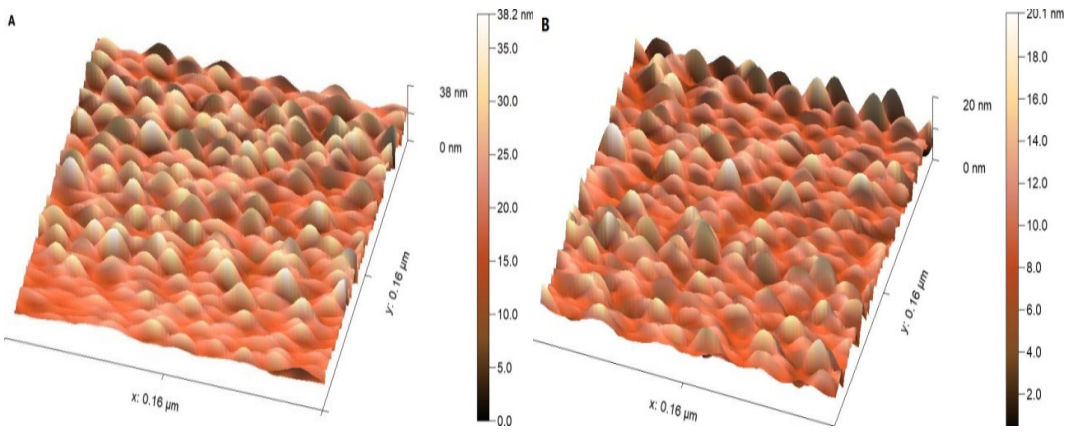

Fig. 8. Atomic Force Microscopy for (A) Y_2O_3 (B) TiO_2.

The absorption spectra of both Y_2O_3 and TiO_2 were analyzed using UV-Vis spectroscopy within the wavelength range of 200-1000 nm, as shown in Fig. (9), to examine the light response of each material and calculate their optical energy gaps. According to the absorption curve, TiO_2 demonstrates absorption begins at 200 nm, and then it gradually increases 600-800 nm. After this peak, the absorption remains relatively high without a sharp decrease due to crystal defects. The energy gap calculated by Tauc plot is 3.3eV indicating the main absorption is in UV range but extended effect 600-800 nm may be related to defects or indirect transitions. The presence of defects such as oxygen vacancies and reduced titanium oxidation states (Ti^{3+}) can lead to additional absorption features beyond the UV range[34]. In contrast, Y_2O_3 shows absorption primarily at wavelengths shorter than 250 nm and increases slowly until it reaches a maximum value of 0.52 a.u at 1000nm, indicating an insulating nature of the material. This behavior is consistent with the calculated energy gap of 5.3, as no light is absorbed in the visible region, but some weak absorption may be shown due to surface effects or impurities [35,36]

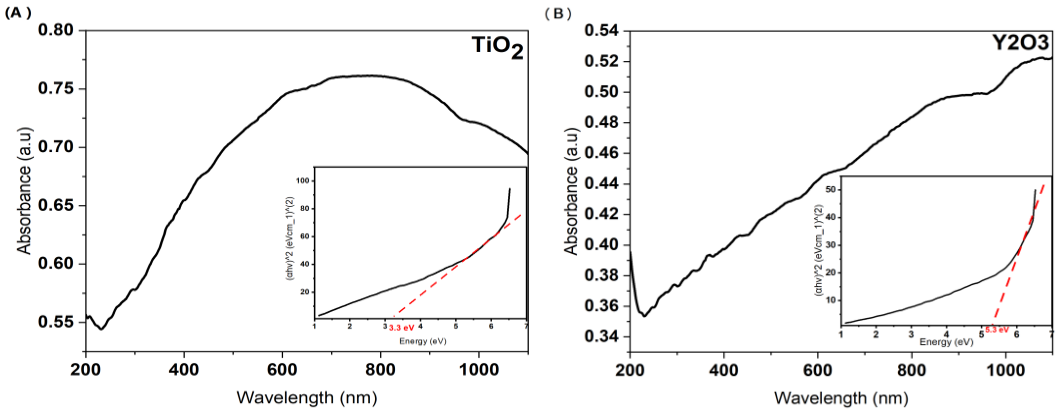

Fig. 9. Ultraviolet-visible absorption spectra and the energy gap of (A)TiO_2 (B) Y_2O_3.

The Fig (10) Shows curves representing the spectral performance of the Ag /TiO_2 /n-Si /Ag photodetector, were represented by Specific Detectiivity (D*) and Responsivity (R).These parameters were calculated using the following relationships[37][38]:

$$R = \frac{I_{ph} - I_d}{PA} \tag{2}$$

$$D* = \frac{R}{\sqrt{\frac{2eI_d}{A}}} \tag{3}$$

where I_{ph} is photocurrent, I_d is dark current, P is power density of incident light, A is effective irradiation area, e is electron charge. It is clear from the figure above that the Ag/TiO_2/n-Si/Ag detector performance is a sharp drop in spectral response (R) after 350 nm, then stability at low values between 450-750 nm, followed by a significant increase at 800-900 nm. This increase is attributed to the fact that TiO_2 with Ag stimulates the surface plasmon, which increases the local electric field and enhances the absorption in the NIR [39,40]. This indicates that the detector responds more strongly at (NIR and UV) range. The specific detectivity (D)* also shows a trend similar to responsivity, the sensitivity high at 350 nm, then decreasing, and rising again at 800-900 nm. We conclude that the Ag/TiO_2/Si/Ag detector suitable for optical detection applications in (NIR and UV) range, while its performance in the visible light range is relatively poor .This means the material absorbs photons more efficiently in (UV and NIR) range , due to the electronic structure or surface effects being optimized in this range rather than visible range [40] [41].

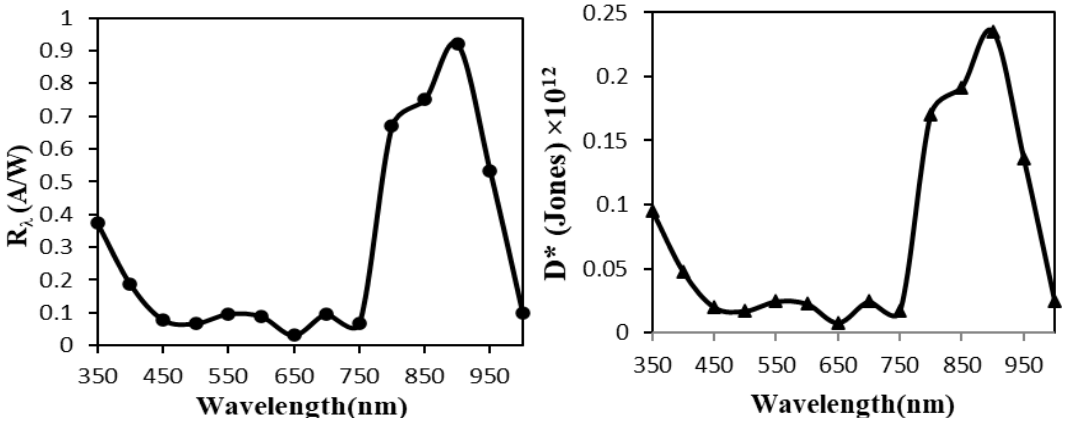

Fig. 10. Responsivity and detectivity a function of wavelength of Ag/ TiO_2/ n-Si / Ag Photoelectric.

Fig. (11) shows the spectral performance curves of Ag/ Y_2O_3 / n-Si / Ag photodetector. The spectral response (R) shows a gradual increase after 450 nm. There are peaks at around 650 nm and 900 nm, indicating a strong response in these regions. This means that the detector operates efficiently in the (Vis and NIR) ranges. The specific detectivity (D)* increases with increasing wavelength, peaking at around 900 nm. The response at short wavelengths is relatively weak but improves significantly after 500 nm. This indicates that the detector has good sensitivity in the visible range. We conclude that the Ag/Y_2O_3/n-Si/Ag photodetector has an improved response compared to Ag/TiO_2/n-Si/Ag photodetector because the Y_2O_3 acts as a medium for storing charge carriers, which reduces recombination and improves the efficiency of charge separation. The spectral response (R) and specific detectivity (D)* appears to be more stable across the wavelengths, making it a better choice for spectral detection applications. The specific detection show improved performance due to the reduction of electronic noise resulting from surface defects, which means that Y2O3 has significantly enhanced the detector efficiency[42][43]. While the Ag/ Y_2O_3 /n-Si/Ag photodetector excels in the visible range, challenges remain in optimizing performance at shorter wavelengths, where sensitivity is comparatively lower. This highlights the ongoing need for advancements in photodetector technology to enhance overall spectral response.

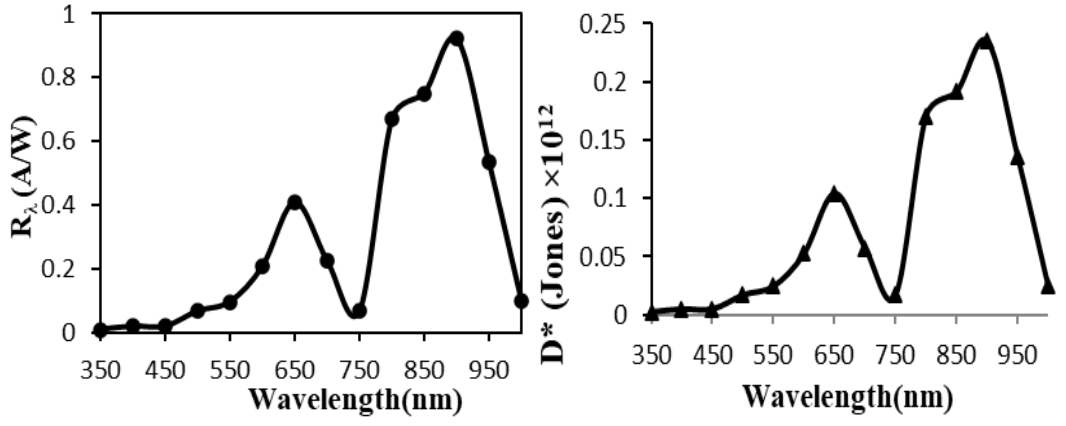

Fig. 11. Responsivity and detectivity a function of wavelength of Ag /Y_2O_3 /n-Si /Ag Photoelectric.

Fig. (12) shows the spectral performance curves of Ag/ TiO_2/ Y_2O_3 / n-Si / Ag photodetector. It was noticed significant improvement in spectral response (R) and specific detectivity (D*) over a wide wavelength range. There are major peaks at ~350nm, ~650 nm and 900

nm, indicating a strong response in these ranges .The specific detectivity D* follows almost the same pattern, with a significant increase at 650 nm, 350 nm and 900 nm. This indicates an improvement in the detection ability in these ranges, which is a good indicator of the sensitivity of the device. There is an improvement in the response at 350 nm compared to Ag/ Y_2O_3 / n-Si / Ag photoelectric, indicating a positive effect of the addition of TiO_2 with Y_2O_3. This detector has a clear advantage in the near-infrared response 800-950 nm and visible 650 nm response making it suitable for detection applications in this range. The response at 350 nm is also improved, which may make it appropriate for dual applications in the (Vis, IR and UV) range. The Ag/ TiO_2/ Y_2O_3 / n-Si / Ag photodetector is the best performance, because is not only enhances the highest spectral response in (Vis-NIR) range but also shows a significant improvement in UV range due to the presence of TiO_2 known for its high to absorb UV rays , reduced recombination, improved absorption sensitivity, and increased photon-to-electron conversion compared to detectors containing TiO_2 or Y_2O_3 alone[42]. Based on these results, the Ag/TiO_2/Y_2O_3/Si/Ag detector is the optimal choice for multi-application sensors.

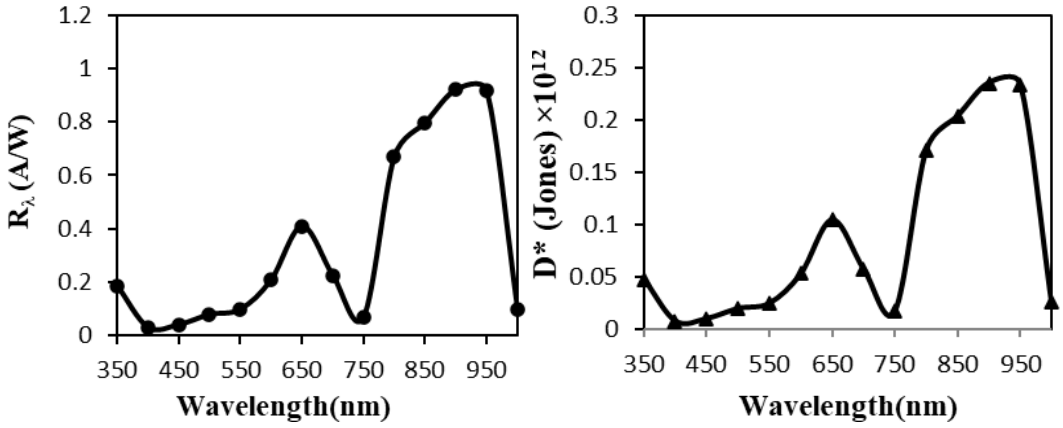

Fig. 12. Responsivity and dtectivity a function of wavelength of Ag/TiO_2 /Y_2O_3 /n-Si /Ag Photoelectric.

5. Conclusion

This study addresses the fabrication and performance evaluation of three nanophotodetectors based on titanium oxide (TiO_2) and yttrium oxide (Y_2O_3) using the laser ablation technique. Three photodetectors, namely: Ag/TiO_2/n-Si/Ag, Ag/TiO_2/Y_2O_3/n-Si/Ag, and Ag/Y_2O_3/n-Si/Ag, were prepared and studied using XRD, FTIR, UV-Vis, AFM, and FESEM techniques to analyze their structural, morphological, and optical properties, in addition to evaluating their electrical properties by measuring the specific detectivity (D*), and Responsivity (R). As per the results, Ag/TiO_2/ Y_2O_3/n-Si/Ag photodetector is more superior and efficient. This is attributed to the spectral response over a wide range of wavelength at (UV-Vis-NIR) range, reduced recombination, improved absorption sensitivity, and increased photon-to-electron conversion compared to detectors containing TiO_2 or Y_2O_3 alone.

It also the cumulative effect of incorporating TiO_2 and Y_2O_3, contributes to reduce the effective energy gap and improved the efficiency of photon absorption and electron transfer. Although TiO_2, showed a good ability to absorb ultraviolet rays but it has weak absorption in the visible spectrum due to its wide energy gap of 3.2 eV when used alone and the high rates of recombination reduced its efficiency in Ag/TiO_2/n-Si/Ag photodetector. As for Ag/ Y_2O_3 /n-Si/Ag, it showed a significant improvement that exceeds the performance of the detector based on TiO_2 alone, which indicates that Y_2O_3 is the main factor responsible for improving the performance of photodetectors at visible range. The results also highlight the effectiveness of laser ablation technology in fabricating high-purity nanomaterials, which directly improves the optical and photoelectric properties of the detectors. These developments can lead to the advancement from a new generation of high-performance photodetectors using potential applications in optical sensing, environmental monitoring, and advanced photonic systems.

References

[1] Z. Li et al., Adv. Funct. Mater., vol. 28, no. 16, p. 1705237, 2018; https://doi.org/10.1002/adfm.201705237

[2] M. A. Darwish, W. Abd-Elaziem, A. Elsheikh, and A. A. Zayed, Nanoscale Adv., 2024; https://doi.org/10.1039/D4NA00214H

[3] Z.-C. Su and C.-F. Lin, 2023 IEEE Silicon Photonics Conference (SiPhotonics), 2023, pp. 1-2; https://doi.org/10.1109/SiPhotonics55903.2023.10141945

[4] K. Singh, N. Berwal, I. Rawal, S. Dahiya, R. Punia, R. Dhar, J. Alloys Compd., vol. 768, pp. 978-990, 2018; https://doi.org/10.1016/j.jallcom.2018.07.303

[5] Y. Ajiki et al., Appl. Phys. Lett., vol. 108, no. 15, 2016; https://doi.org/10.1063/1.4945690

[6] K. S. R. Bapathi, M. F. Abdelbar, W. Jevasuwan, P. H. Borse, S. Badhulika, N. Fukata, Nano Energy, vol. 122, p. 109277, 2024; https://doi.org/10.1016/j.nanoen.2024.109277

[7] C. Ling et al., J. Mater. Chem. C, vol. 10, no. 6, pp. 2049-2059, 2022; https://doi.org/10.1039/D1TC05604B

[8] S. Bansal et al., Nanotechnology, vol. 31, no. 40, p. 405205, 2020; https://doi.org/10.1088/1361-6528/ab9da8

[9] M. Shim, P. Guyot-Sionnest, Nature, vol. 407, no. 6807, pp. 981-983, 2000; https://doi.org/10.1038/35039577

[10] K. R. Chauhan, D. B. Patel, J. Alloys Compd., vol. 792, pp. 968-975, 2019; https://doi.org/10.1016/j.jallcom.2019.04.111

[11] X. Chen et al., ACS Appl. Mater. Interfaces, vol. 9, no. 42, pp. 36997-37005, 2017; https://doi.org/10.1021/acsami.7b09812

[12] T. Xie et al., Appl. Phys. Lett., vol. 107, no. 24, 2015; https://doi.org/10.1063/1.4938129

[13] Sahar Issa Saeed , Maryam Azher Ali , Wedian K. Abad, Ahmed N. Abd, International Journal of Nanoscience ,Vol. 23, No. 2 (2024) 2350063; https://doi.org/10.1142/S0219581X23500631

[14] Z. Long et al., Adv. Electron. Mater., vol. 6, no. 1, p. 1901048, 2020; https://doi.org/10.1002/aelm.201901048

[15] Z. Ma, J. Zhang, H. Lyu, X. Ping, L. Pan, Y. Shi, Metal Oxides for Optoelectronics and Optics-Based Medical Applications, Elsevier, 2022, pp. 117-150; https://doi.org/10.1016/B978-0-323-85824-3.00011-7

[16] K. C. S. Reddy, P. Sahatiya, I. Santos-Sauceda, O. Cortázar, R. Ramírez-Bon, Appl. Surf. Sci., vol. 513, p. 145804, 2020; https://doi.org/10.1016/j.apsusc.2020.145804

[17] X. Ma, L. Tang, Y. Zhang, W. Zuo, K. S. Teng, G. Wu, Infrared Phys. Technol., vol. 139, p. 105305, 2024; https://doi.org/10.1016/j.infrared.2024.105305

[18] Y. S. M. Elzawiei, A. Abdulhameed, M. R. Hashim, M. M. Halim, Opt. Mater. (Amst)., vol. 144, p. 114353, 2023; https://doi.org/10.1016/j.optmat.2023.114353

[19] Y. Shehu, S. A. M. Samsuri, N. M. Ahmed, S. Aslam, Optik (Stuttg)., vol. 304, p. 171784, 2024; https://doi.org/10.1016/j.ijleo.2024.171784

[20] I. H. Kadhim and N. M. Abd-Alghafour, J. Coll. Basic Educ., vol. 30, no. 126, pp. 104-115, 2024; https://doi.org/10.35950/cbej.v30i126.12229

[21] X. Zhang, H. Yang, A. Tang, J. Phys. Chem. B, vol. 112, no. 51, pp. 16271-16279, 2008; https://doi.org/10.1021/jp806820p

[22] C. Liu, P. Huang, W. Wang, M. Tan, F. Fu, Y. Feng, Polymers (Basel)., vol. 15, no. 22, p. 4400, 2023; https://doi.org/10.3390/polym15224400

[23] V. Balaouras, P.-P. Filippatos, A. Chroneos, Mod. Phys. Lett. B, vol. 38, no. 12, p. 2450084, 2024; https://doi.org/10.1142/S0217984924500842

[24] I. Syngelakis et al., The European Conference on Lasers and Electro-Optics, 2023, p. cm_p_12; https://doi.org/10.1109/CLEO/Europe-EQEC57999.2023.10231418

[25] J. Shi, J. Zhang, L. Yang, M. Qu, D. Qi, K. H. L. Zhang, Adv. Mater., vol. 33, no. 50, p. 2006230, 2021; https://doi.org/10.1002/adma.202006230

[26] A. A. Manda et al., Arab. J. Chem., vol. 15, no. 8, p. 104004, 2022; https://doi.org/10.1016/j.arabjc.2022.104004

[27] W. J. Aziz, G. Zuher, R. S. Sabry, Evaluation the effect of the difference of plant extract (oats) from animal extract (chitosan) on the properties of chromium oxide NPs.

[28] L. K. Tinoco Navarro, J. Cihlar, J. Michalicka, J. Kastyl, K. Castkova, Catal. Letters, vol. 154, no. 5, pp. 2422-2442, 2024; https://doi.org/10.1007/s10562-023-04489-7

[29] A. Sanchez-Martinez et al., Mater. Res. Express, vol. 6, no. 8, p. 85085, 2019; https://doi.org/10.1088/2053-1591/ab21e8

[30] S. Ahmad, M. Faizan, S. Ahmad, M. Ikram, AIP Conference Proceedings, 2018, vol. 1942, no. 1; https://doi.org/10.1063/1.5028644

[31] S. Kumar et al., J. Mol. Struct., vol. 1302, p. 137463, 2024; https://doi.org/10.1016/j.molstruc.2023.137463

[32] D. Jacoba, P. Ranaa, A. Ashoka, P. Lasyaa, S. Yadava, SSRN 5078969, 2024; https://doi.org/10.2139/ssrn.5078969

[33] J. Park, A. B. Tesler, E. Gongadze, A. Iglič, P. Schmuki, A. Mazare, ACS Appl. Mater. Interfaces, vol. 16, no. 4, pp. 4430-4438, 2024; https://doi.org/10.1021/acsami.3c16033

[34] H. C. Vasconcelos, M. Meirelles, R. Özmenteş, A. Korkut, Coatings, vol. 15, no. 1, p. 19, 2024; https://doi.org/10.3390/coatings15010019

[35] A. Zatsepin et al., Nanomaterials, vol. 12, no. 15, p. 2726, 2022; https://doi.org/10.3390/nano12152726

[36] Abad, Wedian K.;• Abd, Ahmed N.;• Habubi, Nadir Fadhil , Synthesis of Ag2O Nanoparticles via Fresh Pomegranate Peel Extract for Bioapplications , Nano Biomedicine and EngineeringOpen AccessVolume 15, Issue 4, Pages 363 – 3682023., https://www.sciopen.com/article/10.26599/NBE.2023.9290032

[37] M. A. Al-Azzawi, M. A. Ali, W. K. Abad, J. Opt., pp. 1-10, 2024; https://doi.org/10.1007/s12596-024-01718-z

[38] Habubi, Nadir F.,Ismail, Raid A, Abd, Ahmed N. ,Hamoudi, Walid K. Iimproved photoresponse of porous silicon photodetectors by embedding CdSe nanoparticles , Indian Journal of Pure and Applied Physics 53, Issue 11, (2015) 718 – 724, http://op.niscair.res.in/index.php/IJPAP/article/view/8461

[39] S. A. Abdulgafar, M. A. Ibrahem, Y. M. Hassan, Opt. Mater. (Amst)., vol. 147, p. 114601, 2024; https://doi.org/10.1016/j.optmat.2023.114601

[40] Shaymaa N. Ismail, Ehab.m. Ali, Bahaa Jawad Alwan, Ahmed N. Abd, International Conference on Science and Engineering of Materials - ICSEM 2021 Part I .February (2022) 2100312; https://doi.org/10.1002/masy.202100312

[41] E. Abubakr, A. Abadi, M. Oshita, S. Saito, T. Kan, Opt. Mater. (Amst)., vol. 150, p. 115175, 2024; https://doi.org/10.1016/j.optmat.2024.115175

[42] H. Jia et al., J. Am. Ceram. Soc., vol. 105, no. 8, pp. 5252-5261, 2022; https://doi.org/10.1111/jace.18501

[43] Obaid, Maithm A., Hellal Harbi, Khalid , Abd, Ahmed N. Study the effect of antibacterial on the chemically prepared copper oxide , Materials Today: Proceedings, 47, (2021) 6006 – 6010https://www.sciencedirect.com/science/article/abs/pii/S2214785321034799, ,